

LETTER • OPEN ACCESS

## Long-range transport of Siberian wildfire emissions reduces $\text{NO}_x$ in downwind regions

To cite this article: Dongjin Kim *et al* 2025 *Environ. Res. Lett.* **20** 124053

View the [article online](#) for updates and enhancements.

You may also like

- [Circumpolar spatio-temporal patterns and contributing climatic factors of wildfire activity in the Arctic tundra from 2001–2015](#)  
Arif Masrur, Andrey N Petrov and John DeGroot
- [Associations between fine particulate matter and in-home blood pressure during the 2022 wildfire season in Western Montana, USA](#)  
Ethan S Walker, Taylor Stewart, Rajesh Vedanthan *et al.*
- [A review of the effects of wildfire smoke on the health and behavior of wildlife](#)  
O V Sanderfoot, S B Bassing, J L Brusa *et al.*



The Electrochemical Society  
Advancing solid state & electrochemical science & technology



**249th  
ECS Meeting**  
May 24-28, 2026  
Seattle, WA, US  
*Washington State  
Convention Center*

# Spotlight Your Science

***Submission deadline:  
December 5, 2025***

**SUBMIT YOUR ABSTRACT**

ENVIRONMENTAL RESEARCH  
LETTERS

## LETTER

## OPEN ACCESS

## RECEIVED

14 July 2025

## REVISED

12 October 2025

## ACCEPTED FOR PUBLICATION

27 November 2025

## PUBLISHED

4 December 2025

Original content from this work may be used under the terms of the [Creative Commons Attribution 4.0 licence](#).

Any further distribution of this work must maintain attribution to the author(s) and the title of the work, journal citation and DOI.

Long-range transport of Siberian wildfire emissions reduces NO<sub>x</sub> in downwind regionsDongjin Kim<sup>1,2</sup> , Yunsoo Choi<sup>3</sup>, Hyun Cheol Kim<sup>4,5</sup> , Arman Pouyaei<sup>6</sup> , Jaehyeong Park<sup>1</sup> , Jeonghyeok Moon<sup>7</sup> , Chae-Yeong Yang<sup>1,2</sup> , Cheol-Hee Kim<sup>2,8,9</sup> and Wonbae Jeon<sup>2,8,\*</sup> <sup>1</sup> Division of Earth Environmental System, Pusan National University, Busan 46241, Republic of Korea<sup>2</sup> BK21 School of Earth and Environmental Systems, Pusan National University, Busan 46241, Republic of Korea<sup>3</sup> Department of Earth and Atmospheric Sciences, University of Houston, Houston, TX 77204, United States of America<sup>4</sup> Air Resources Laboratory, National Oceanic and Atmospheric Administration, College Park, MD 20740, United States of America<sup>5</sup> Cooperative Institute for Satellite Earth System Studies, University of Maryland, College Park, MD 20742, United States of America<sup>6</sup> Program in Atmospheric and Oceanic Sciences, Princeton University, Princeton, NJ 08540, United States of America<sup>7</sup> Environmental Planning Institute, Seoul National University, Seoul 08826, Republic of Korea<sup>8</sup> Department of Atmospheric Sciences, Pusan National University, Busan 46241, Republic of Korea<sup>9</sup> Institute of Environmental Studies, Pusan National University, Busan 46241, Republic of Korea

\* Author to whom any correspondence should be addressed.

E-mail: [wbyeon@pusan.ac.kr](mailto:wbyeon@pusan.ac.kr)**Keywords:** wildfire, anthropogenic NO<sub>x</sub>, O<sub>3</sub>, VOCs, FINN, CMAQSupplementary material for this article is available [online](#)

## Abstract

Wildfires are widely known to increase atmospheric pollutant concentrations, deteriorating air quality. However, several studies have reported that wildfires can also reduce the concentrations of certain gaseous species. This study investigated the impacts of smoke plumes from wildfires that occurred in late July 2014 in Siberia, Russia, on downwind gaseous pollutants such as carbon monoxide (CO), nitrogen oxides (NO<sub>x</sub>), volatile organic compounds (VOCs), and ozone (O<sub>3</sub>). The Community Multi-scale Air Quality model was employed for air quality simulations, and wildfire emissions were obtained from the Fire INventory from the National Center for Atmospheric Research. Wildfire-induced CO, VOCs, and O<sub>3</sub> were transported to Northeast China (NEC), the Yellow Sea (YS), and the Korean Peninsula (KP), resulting in elevated pollutant levels in these downwind regions. Interestingly, despite the transport of plumes, surface-level NO<sub>x</sub> concentrations over NEC, YS, and KP even decreased. Such reductions were not evident near the Siberian source areas but became apparent after the plumes reached the NEC region. In these regions, NO was converted through reactions with wildfire-induced VOCs (84.54%) and NO<sub>3</sub> radicals (13.18%), while NO<sub>2</sub> was primarily transformed into NO<sub>3</sub> radicals via reactions with O<sub>3</sub> (90.08%) or into organic nitrates through reactions with VOCs (9.92%). We found that the observed conversions in NO<sub>x</sub> concentrations were attributable to anthropogenic sources, as the conversion patterns varied depending on the level of anthropogenic NO<sub>x</sub> emissions in the sensitivity experiments. These results suggest that wildfire-driven NO<sub>x</sub> concentration changes in downwind regions cannot be fully explained by wildfire emissions alone. This study underscores the importance of accurately characterizing anthropogenic emission sources in regions affected by smoke plume transport to predict changes in gaseous pollutant concentrations following wildfire events. We expect that this study will enhance future wildfire-related research by improving the prediction of the spatial distribution and atmospheric behavior of gaseous pollutants.

## 1. Introduction

In late July 2014, numerous wildfires occurred across the Siberian region of Russia (Li *et al* 2017, Zhu *et al* 2019). These wildfires are one of the primary contributors to global air pollution, emitting substantial amounts of gaseous pollutants such as carbon monoxide (CO), nitrogen oxides (NO<sub>x</sub>), sulfur dioxide (SO<sub>2</sub>), ammonia (NH<sub>3</sub>), and volatile organic compounds (VOCs), as well as particulate matter (Urbanski *et al* 2008, Dreessen *et al* 2016). NO<sub>x</sub> and VOCs contribute to the formation of ozone (O<sub>3</sub>) through photochemical reactions in the atmosphere (Baylon *et al* 2015, Kim *et al* 2022a), and NO<sub>x</sub>, SO<sub>2</sub>, and NH<sub>3</sub> act as precursors of particulate matter, thereby deteriorating air quality (Majdi *et al* 2019, Li *et al* 2023). According to Jung *et al* (2016), smoke plumes induced by the Siberian wildfires were transported more than 3000 km to downwind regions including Mongolia, Northeast China (NEC), and the Korean Peninsula (KP). These smoke plumes caused high PM<sub>2.5</sub> concentrations in NEC, exceeding 100 µg m<sup>-3</sup>, which is approximately 3–6 times higher than the background levels (Li *et al* 2017). The plumes were continuously transported through China and contributed to increased PM<sub>2.5</sub> concentrations in Daejeon, South Korea (Jung *et al* 2016). This indicates that air pollutants emitted from Siberian wildfires can undergo long-range transport to regions such as China, the KP, and Japan under northerly or northwesterly synoptic meteorological conditions, potentially leading to air quality deterioration (Jeong *et al* 2008, Ikeda *et al* 2015, Trieu *et al* 2023).

Previous studies have primarily focused on analyzing the contribution of the 2014 Siberian wildfires to the increase in PM<sub>2.5</sub> concentrations. However, several studies have reported that the concentrations of certain gaseous pollutants in downwind regions can exhibit a decreasing pattern. Kang *et al* (2014) found that the Quebec wildfire plumes increased O<sub>3</sub> concentrations over major cities and rural areas, while O<sub>3</sub> concentrations decreased near the wildfire spots due to NO<sub>x</sub> titration effects. Souri *et al* (2017) showed that O<sub>3</sub> and VOCs induced by wildfires in the U.S. were transported into urban areas, resulting in reductions in regional NO concentrations through atmospheric chemical reactions. These gaseous pollutants from wildfires are involved in complex chemical reactions in the atmosphere, which can lead to reductions in the concentrations of certain species depending on the characteristics of the regions affected by the transported smoke plumes. Therefore, the impact of emissions from the Siberian wildfires on gaseous pollutant concentrations in downwind regions, including China and the KP, warrants further investigation.

In this study, we analyzed the concentration changes of major gaseous pollutants emitted from wildfires that occurred in late July 2014 in Siberia,

Russia, as smoke plumes were transported downwind. The analysis was performed using the three-dimensional photochemical model Community Multi-scale Air Quality (CMAQ) and high-resolution wildfire emissions data obtained from Fire INventory from National Center for Atmospheric Research (FINN). In addition, to investigate the mechanisms of chemical reactions involved in the production and loss of gaseous pollutants, we employed the integrated reaction rate (IRR) module provided by the CMAQ model.

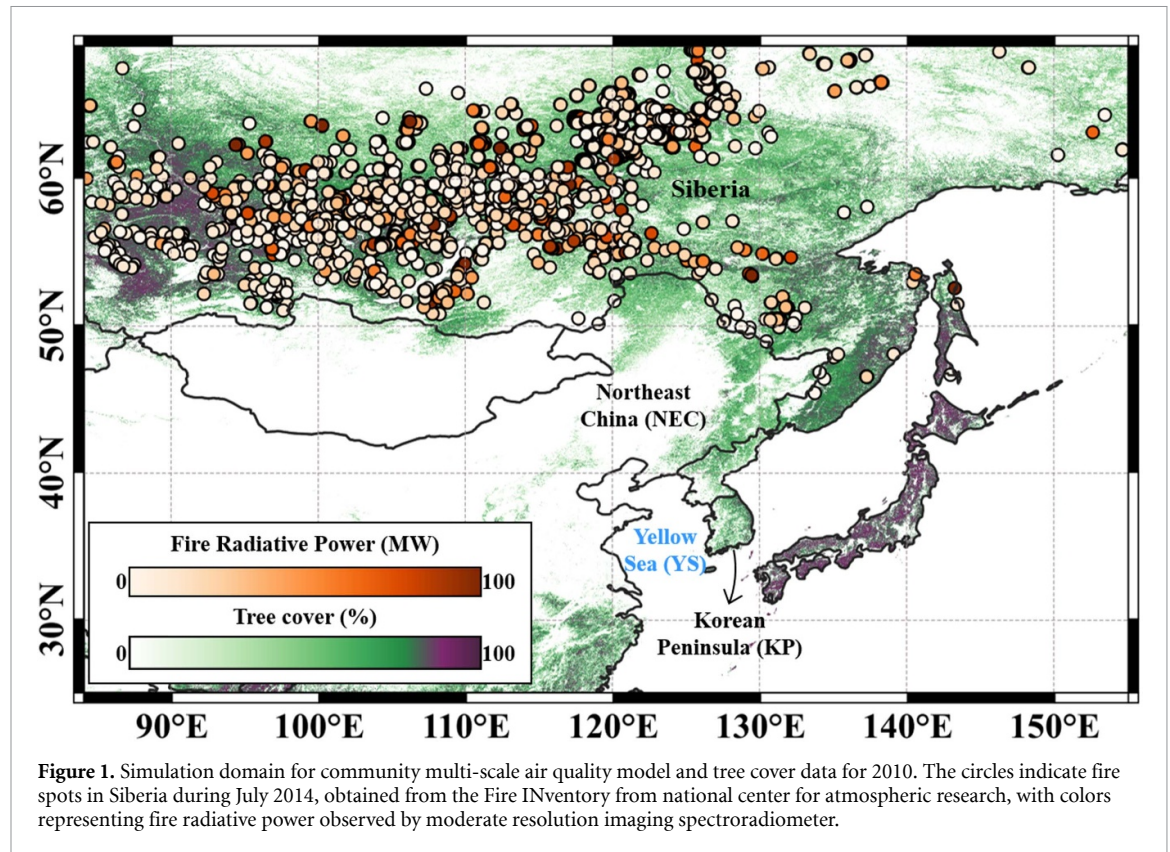
## 2. Methodology

### 2.1. Numerical simulation setup

We utilized the CMAQ (v5.3.2, Appel *et al* 2021) model, developed by the U.S. Environmental Protection Agency, to investigate the changes in gaseous pollutant concentrations during the transport of smoke plumes from the Siberian wildfires in July 2014. The simulation domain was configured to encompass the Siberian region and Northeast Asia, with a spatial resolution of 27 km. According to the forest cover database by Hansen *et al* (2013), the Siberian region within the domain is densely covered with trees, and substantial wildfires occurred in July 2014 (figure 1).

Meteorological input data for the CMAQ model were generated using the Weather Research and Forecasting (WRF) (v4.1.1, Skamarock *et al* 2019) and the Meteorology–Chemistry Interface Processor (v5.1, Otte and Pleim 2010). The initial and boundary conditions for the WRF model were derived from ERA5 data provided by the European Centre for Medium-Range Weather Forecasts, with a horizontal resolution of 0.25° × 0.25° and a temporal interval of 6 h. The WRF model was configured with the following physical schemes: the WSM 3-class simple ice scheme for microphysics, the RRTM scheme for long-wave radiation, the Dudhia scheme for short-wave radiation, the Monin–Obukhov similarity scheme for the surface layer, the Noah land surface model, the YSU scheme for planetary boundary layer processes, and the Kain–Fritsch (new Eta) scheme for cumulus parameterization. For the CMAQ model, daily average hemispheric CMAQ outputs from the CMAS data warehouse were utilized to minimize errors in initial and boundary conditions during the simulation (Appel *et al* 2021, Mazzeo *et al* 2022). Anthropogenic emission input data were generated using the Emissions Database for Global Atmospheric Research (v6.1, Crippa *et al* 2022), while biogenic emissions were estimated using the Model of Emissions of Gases and Aerosols from Nature (v2.1, Guenther *et al* 2012). Wildfire emissions for the Siberian region were extracted from the FINN (v2.5, Wiedinmyer *et al* 2023) data, which provides daily high-resolution biomass burning emissions data. The chemical mechanisms CB6r3 and





AERO7 were applied in the CMAQ model for the gaseous and aerosol phases. The simulation was conducted from 13 July–9 August 2014, when Siberian wildfire emissions were transported to Northeast Asia. The detailed configurations of the WRF and CMAQ models used in this study are presented in tables S1 and S2, respectively.

To evaluate the contributions of chemical reactions to the production and loss of gaseous pollutants induced by the Siberian wildfires, we utilized the IRR module provided by the CMAQ model (Byun and Ching 1999, Park *et al* 2021, 2022, Jo *et al* 2023, Kim *et al* 2024). The IRR quantifies the contributions of individual chemical reactions in the mechanism used in the CMAQ simulation, allowing for the identification of precursor species involved in the formation and destruction processes of specific materials.

## 2.2. Vertical allocation of wildfire emissions

The smoke plume height of pollutants emitted from wildfires is significantly influenced by various factors, including meteorological conditions and terrain in the region where the wildfire occurred (Val Martin *et al* 2010, Paugam *et al* 2016). Accordingly, the vertical allocation of wildfire emissions in the CMAQ model is critical for improving the accuracy of air quality simulation results (Jeon *et al* 2018, Kim *et al* 2022a). Numerous studies have been conducted to determine the most suitable plume height for the vertical distribution of wildfire emissions (Bieser *et al* 2011, Raffuse *et al* 2012, Sofiev *et al* 2012, Huang

*et al* 2023). In this study, we employed the method proposed by Sofiev *et al* (2012) and Pouyaei *et al* (2025) to estimate the smoke plume height of Siberian wildfires. This method requires input parameters: the height of the atmospheric boundary layer (ABL) ( $H_{abl}$ ), fire radiative power (FRP), and Brunt–Väisälä frequency ( $N$ ), to calculate the injection height ( $H_p$ ). The detailed equation is as follows:

$$H_p = \alpha H_{abl} + \beta \left( \frac{FRP}{P_{f0}} \right)^\gamma \exp \left( -\frac{\delta N_{FT}^2}{N_0^2} \right).$$

Here,  $P_{f0}$  represents the reference FRP ( $\approx 10^6$  W),  $N_0$  is the reference  $N$  ( $N_0^2 \approx 2.5 \times 10^{-4} \text{ s}^{-2}$ ),  $N_{FT}$  denotes the  $N$  in the free troposphere. The constants are defined as follows:  $\alpha$  is the portion of the ABL that is freely crossed ( $\alpha = 0.24$ ),  $\beta$  represents the weighting factor for the fire intensity ( $\beta = 170$  m),  $\gamma$  indicates the degree of power-law dependence on FRP, and  $\delta$  characterizes the dependence on FT stability ( $\delta = 0.6$ ).

For the calculation of injection heights of the Siberian wildfires, we used FRP data observed by the moderate resolution imaging spectroradiometer onboard the National Aeronautics and Space Administration (NASA)'s Terra and Aqua satellites at a spatial resolution of 1 km. This resolution is identical to that of the FINN dataset; however, discrepancies exist in the locations of the detected fire points between the two datasets. Therefore, wildfire emissions were allocated to the nearest CMAQ grid cell, and the FRP value observed at the closest location

and time was used to calculate the injection height. The meteorological variables required for calculating  $H_{abl}$  and  $N$  were derived from simulation results performed using the WRF model in this study.

Since the FINN (v2.5) provides wildfire emissions as daily data, each fire was assumed to have occurred entirely on the day it was observed. We conducted an experiment including wildfire emissions (SIB) by uniformly distributing the Siberian wildfire emissions over the observed day and the corresponding injection heights for each fire event. This SIB simulation was compared with a baseline experiment without wildfire emissions (BASE) to quantitatively assess the air quality changes caused by the Siberian wildfires.

### 2.3. Ground and satellite observation data

To assess the accuracy of the numerical simulation results from the WRF and CMAQ models used in this study, ground-based meteorological observation data (94 sites in South Korea and 83 sites in China) and air quality observation data (316 sites in South Korea and 754 sites in China) within the domain were utilized. The evaluation was performed for surface temperature, wind speed, and  $O_3$  concentration. The statistical parameters include root mean squared error (RMSE) and mean bias error (MBE) to evaluate the differences between observations and model simulations, and index of agreement (IOA) to assess the model's accuracy. The statistical metrics used for the verification are as follows,

$$RMSE = \sqrt{\frac{1}{N} \sum_{i=1}^N (M_i - O_i)^2}$$

$$MBE = \frac{1}{N} \sum_{i=1}^N (M_i - O_i)$$

$$IOA = 1 - \frac{\sum_{i=1}^N (M_i - O_i)^2}{\sum_{i=1}^N (|M_i - \bar{O}| + |O_i - \bar{O}|)^2}$$

In the above equations,  $N$  represents the number of observation data,  $M$  denotes the modeled values,  $O$  indicates the observed values, and  $\bar{O}$  is the mean of the observed values.

$NO_x$  and VOCs are key gaseous pollutants that play important roles in forming and destroying  $O_3$  in the atmosphere. Therefore, we conducted an additional evaluation of the model performance by comparing CMAQ-simulated concentrations of  $NO_2$  and formaldehyde with satellite observations. The Ozone Monitoring Instrument (OMI) onboard NASA's Aura satellite provides observations of  $NO_2$  and formaldehyde column concentrations (Chance 2007, Krotkov *et al* 2024). To align the OMI level 2 observational data with the CMAQ model grid, the oversampling techniques proposed by Sun *et al* (2018) were applied. The  $NO_2$  and formaldehyde simulated by the CMAQ

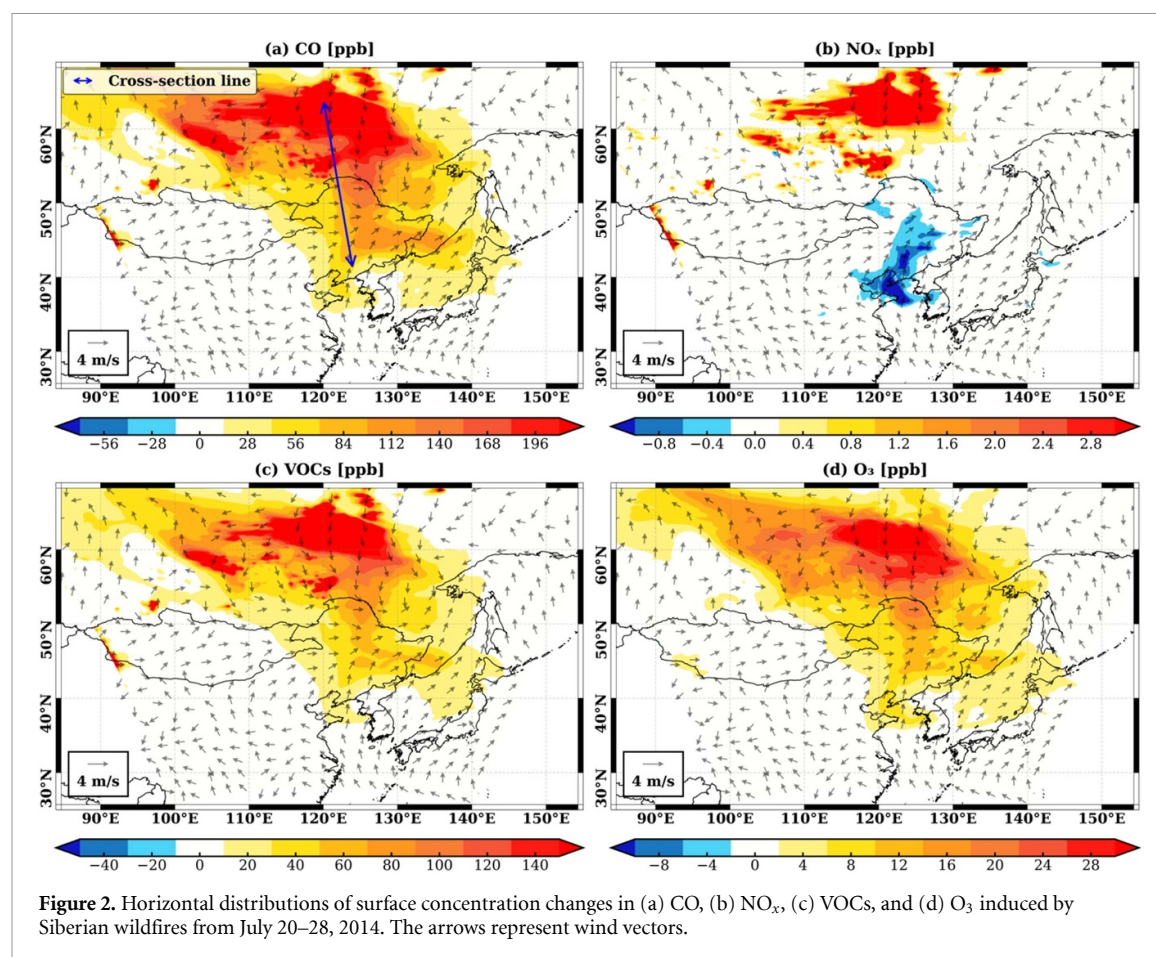
model were converted into column densities for comparison with satellite observations. Through this process, we evaluated the model performance. The simulated temperature, wind speed, and  $O_3$  well captured the temporal variability observed at surface monitoring sites in South Korea and China (figure S1). In addition, the CMAQ model successfully reproduced the spatial distributions of  $NO_2$  and formaldehyde emitted from anthropogenic, biogenic, and wildfire sources (figure S2).

We additionally assessed the simulation performance of the SIB experiment, which includes wildfire emissions, for the spatial distributions of CO,  $NO_2$ , and  $O_3$  (figure S3). The CMAQ-simulated  $NO_2$  and  $O_3$  generally reproduced the observed spatial distributions well, whereas CO was substantially underestimated. This is considered to be attributable to the underestimation of CO emissions in global anthropogenic emissions inventories, including EDGAR, as highlighted in previous studies (Feng *et al* 2020, Tang *et al* 2022, Kim *et al* 2022b, Xie *et al* 2025). Overall, these evaluation results demonstrate that the model effectively captures not only the observed temporal variability but also the horizontal and vertical distributions.

## 3. Results and discussion

### 3.1. Concentration changes in gaseous pollutants due to Siberian wildfires

During the simulation period, Siberian wildfires emitted large amounts of gaseous pollutants into the atmosphere (table S3). These pollutants increased CO and  $O_3$  concentrations in the downwind regions, including NEC and South Korea. To quantify the wildfire impacts, we compared observations from wildfire plume-affected sites (234 in China and 144 in South Korea) with the simulated results from the BASE and SIB experiments. The wildfire influence was evident between 24 July and 30, 2014, during which the observed CO concentrations averaged 750.99 ppb, representing an increase of approximately 265.01 ppb compared to unaffected days (485.99 ppb). The CMAQ simulations showed that CO concentrations increased by up to 155.33 ppb, with an average increase of 56.53 ppb in the SIB experiment compared with the BASE experiment (figure S4(a)). Although the wildfire plume slightly elevated CO levels over these downwind regions, the model did not adequately reproduce the observed variability, primarily due to the underestimation of anthropogenic CO emissions, as discussed in section 2.3. In contrast, the model effectively captured the wildfire-induced enhancement of  $O_3$  concentrations (figure S4(b)). During the wildfire-affected days, the BASE experiment tended to underestimate  $O_3$  concentrations, whereas the SIB experiment successfully reproduced the observed increasing trend, thereby improving the overall model performance (table S4).



To quantitatively assess the impact of wildfire emissions on major atmospheric gaseous pollutants, we examined the horizontal distributions of surface concentration changes for CO, the most abundantly emitted species, along with the primary O<sub>3</sub> precursors, NO<sub>x</sub> and VOCs (Mun *et al* 2023, Park *et al* 2024), as well as O<sub>3</sub>. Concentration changes were calculated as the difference between the SIB and BASE experiments (i.e. SIB minus BASE) and averaged over July 20–28, 2014, when smoke plumes were transported to downwind regions, including China and the KP.

In the Siberian region with widespread fire spots, concentrations of CO, NO<sub>x</sub>, and VOCs increased due to direct emissions from wildfires (figures 2(a)–(c)). These species acted as precursors, enhancing secondary chemical formation processes, thereby increasing O<sub>3</sub> concentrations (figure 2(d)). CO, VOCs, and O<sub>3</sub> were transported southward by northerly winds associated with synoptic systems, including low-pressure systems and typhoons (figure S6), leading to elevated concentrations over NEC, the Yellow Sea (YS), and the KP. However, NO<sub>x</sub> exhibited a distinct distribution pattern. In contrast to other species, NO<sub>x</sub> concentrations decreased (figure 2(b)), consistent with findings by Sourin *et al* (2017), which reported downwind NO<sub>x</sub> reductions during wildfire events. This behavior deviates from the typical pattern of elevated

pollutant levels during wildfire episodes, warranting further comprehensive analysis.

We examined the vertical concentration profiles of each pollutant along the cross-section line representing the transport pathway (figure 2(a)), as presented in figure 3. Similar to the surface distributions, the concentrations of CO, VOCs, and O<sub>3</sub> increased over the wildfire source regions in Siberia and extended vertically to the upper levels of the ABL (figures 3(a), (c) and (d)). These pollutants were subsequently transported toward the NEC region, with their concentrations gradually diminishing along the transport pathway. NO<sub>x</sub> emitted from the wildfires was also transported to downwind regions. However, when the smoke plume reached the NEC, NO<sub>x</sub> concentrations decreased near the surface within the ABL, consistent with the horizontal distribution (figure 3(b)). This indicates that surface-level NO<sub>x</sub> concentrations in the NEC region were not driven by wildfire-emitted NO<sub>x</sub>, but rather by the chemical loss processes. It also highlights that changes in NO<sub>x</sub> concentrations in downwind regions, located far from the wildfire sources, cannot be explained solely by direct NO<sub>x</sub> emissions from the wildfires. Accordingly, we aim to investigate why reductions in NO<sub>x</sub> concentrations were observed only in specific regions, such as NEC, YS, and KP, during the Siberian wildfire events. To



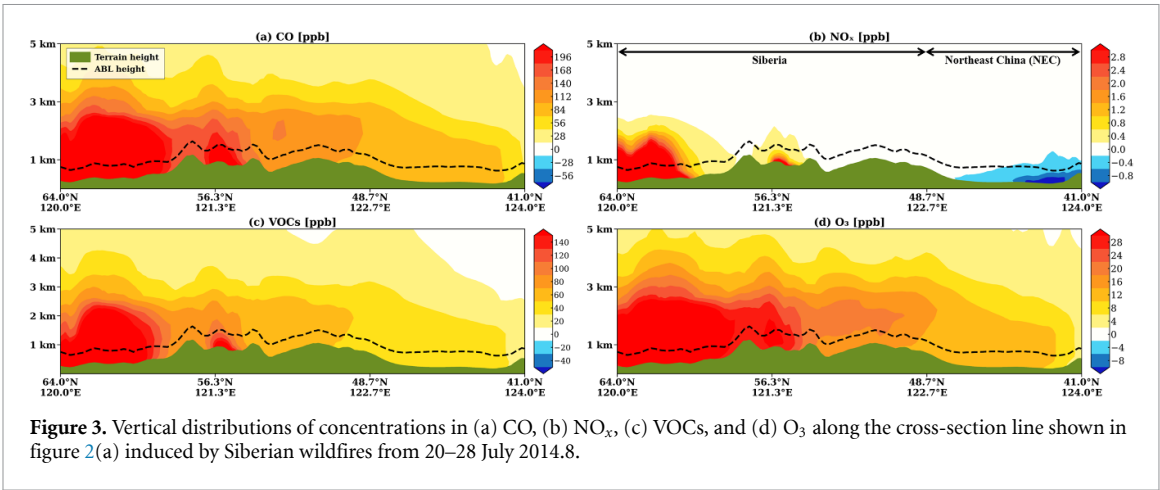


**Figure 3.** Vertical distributions of concentrations in (a) CO, (b) NO<sub>x</sub>, (c) VOCs, and (d) O<sub>3</sub> along the cross-section line shown in figure 2(a) induced by Siberian wildfires from 20–28 July 2014.8.

**Table 1.** Descriptions of two phases classified based on changes in pollutant concentrations from 20–28 July 2014.

Period	Dates	Description
EP1	20–21 July 2014	Transport of pollutants from Siberian wildfires to downwind regions
EP2	22–28 July 2014	Decrease in NO <sub>x</sub> concentrations in downwind regions

better understand the underlying mechanisms, it is essential to examine the transport processes of the wildfire smoke plumes thoroughly. For this purpose, we performed a focused analysis for the period of July 20–28, during which wildfire emissions were transported to NEC, YS, and KP.

3.2. Analysis of NO<sub>x</sub> concentration changes during the transport of the wildfire smoke plume

During the Siberian wildfire events, a decrease in NO<sub>x</sub> concentrations was observed in the downwind regions, including NEC, YS, and KP. To investigate this phenomenon, we divided the analysis period into two phases. The first phase (EP1) corresponds to the period when wildfire-emitted pollutants were transported to the downwind regions. The second phase (EP2) encompasses the period during which reductions in NO<sub>x</sub> concentrations were observed in those regions (table 1). For a more detailed analysis, changes in NO and NO<sub>2</sub> concentrations were examined separately. During EP1, both NO and NO<sub>2</sub> concentrations increased in the Siberian region as a direct result of wildfire emissions (figures 4(a) and (b)). These elevated concentrations near the wildfire source regions reflect the immediate impacts of the fires. NO<sub>x</sub> was subsequently transported toward NEC by northerly winds, without any notable decrease in either NO or NO<sub>2</sub> concentrations along the transport pathway. In EP2, CO, VOCs, and O<sub>3</sub> were continuously transported from Siberia to the NEC, YS, and KP regions (figure S7), leading to increases of up to 149.30 ppb, 73.3 ppb, and 16.62 ppb, respectively, within the analysis area shown in figures 4(c) and (d) (figure S8). However, despite the continuous NO<sub>x</sub> emissions from the Siberian wildfires, an anomalous

pattern was observed in these regions. The decrease in NO<sub>x</sub> concentrations was mainly observed during the daytime (figure S8), with the maximum reduction reaching approximately −4.07 ppb. Notably, the decline in NO<sub>2</sub> concentrations was more pronounced than that of NO, suggesting that NO<sub>2</sub> played a more significant role in the overall reduction of NO (figures 4(c) and (d)).

This decreasing pattern in NO<sub>x</sub> concentrations was not observed during EP1, when the wildfire smoke plume was being transported within the Siberian region. Interestingly, a reduction occurred only during EP2, after the plume arrived in NEC. This suggests that a series of chemical reactions leading to surface-level NO<sub>x</sub> depletion was triggered following the transport of wildfire smoke to NEC. To better understand the spatial distribution of NO depletion, it is essential to identify the chemical reactions involving wildfire-emitted species that contributed to the observed reductions and to determine the sources responsible for the reduced NO. To this end, we analyzed all NO-related reactions in the CMAQ model and quantified the contributions of individual reactions to NO and NO<sub>2</sub> concentrations using the IRR module.

3.3. Investigation of chemical mechanisms driving NO<sub>x</sub> reduction

We conducted an IRR analysis over the rectangular area indicated in figures 4(c) and (d) to investigate the NO<sub>x</sub> concentration reductions observed in NEC, YS, and KP during the EP2 period. All reactions associated with the loss of NO and NO<sub>2</sub>, as defined in the chemical mechanism used in this study (CB6r3-AERO7), were considered, and

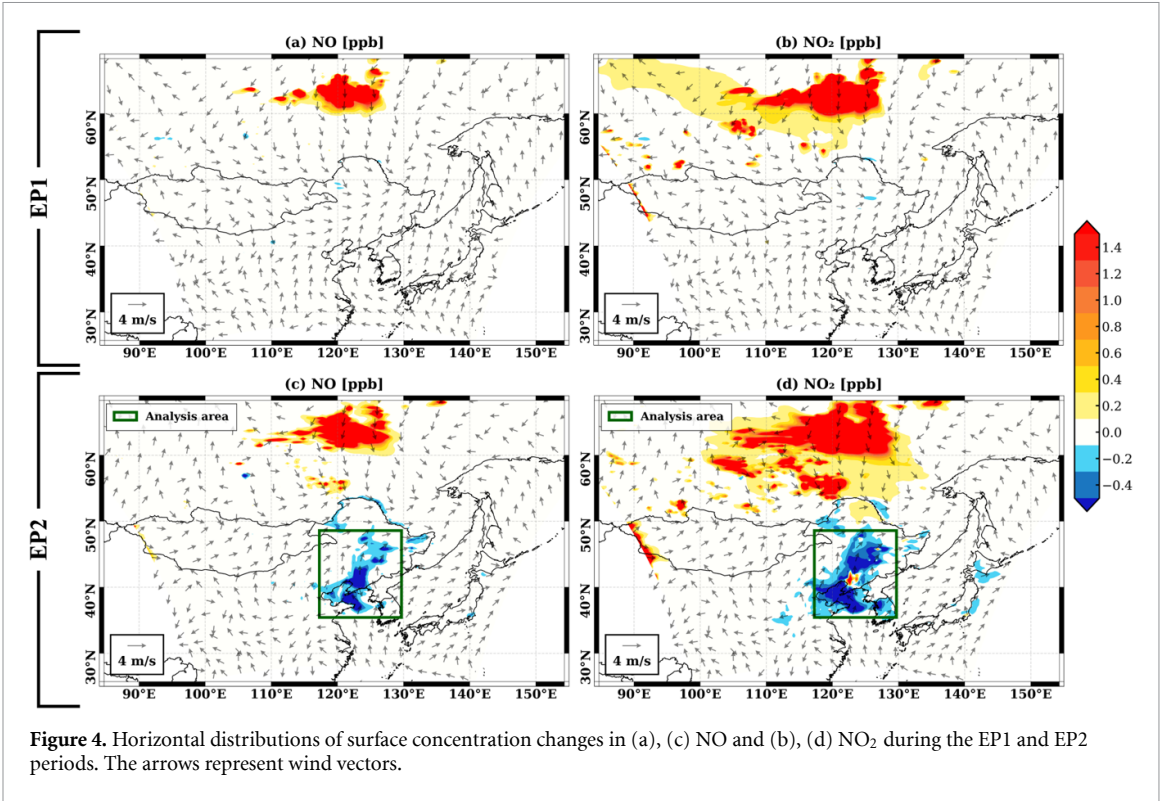


**Table 2.** Contributions of major chemical reactions to the reductions in NO and NO<sub>2</sub> concentrations within the analysis area depicted in figures 4(c) and (d) during the EP2 period.

NO loss reactions	
VOCs + NO = NO <sub>2</sub> + VOCs oxidation products	84.54%
NO <sub>3</sub> + NO = NO <sub>2</sub>	13.18%
NO <sub>2</sub> loss reactions	
O <sub>3</sub> + NO <sub>2</sub> = NO <sub>3</sub>	90.08%
VOCs + NO <sub>2</sub> = Organic nitrates	9.92%

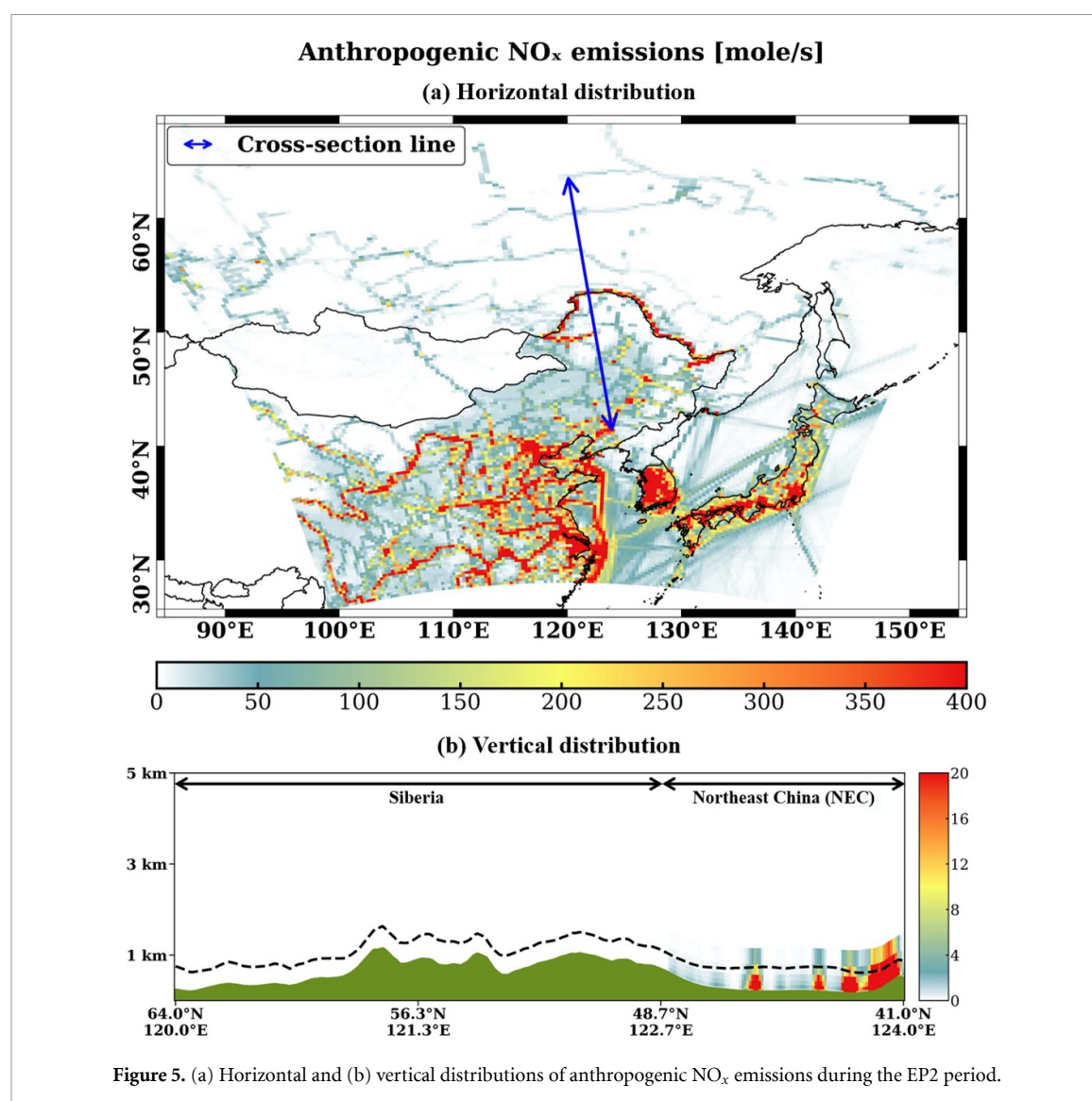
the major contributing reactions are presented in table 2.

In the analysis region, NO was primarily converted through reactions with VOCs (84.54%) and NO<sub>3</sub> radicals (13.18%), with 93.84% of the total NO conversion occurring during daytime. Meanwhile, NO<sub>2</sub> was predominantly transformed via reactions with O<sub>3</sub> (90.08%) and also reacted with VOCs to form organic nitrates (9.92%). These NO<sub>2</sub> transformation processes occurred 68.27% during daytime and 37.73% at night, with the main reaction pathways being the same under both day and night conditions. Through these mechanisms, wildfire-induced VOCs, O<sub>3</sub>, and NO<sub>3</sub> radicals were transported to NEC, YS, and KP, where they reacted with NO<sub>x</sub> and facilitated its chemical conversion. A notable result is that, even though wildfires emitted NO<sub>x</sub> into the atmosphere and the smoke plume was transported to the NEC, YS, and KP regions, NO<sub>x</sub> concentrations decreased in these areas. This indicates that the NO<sub>x</sub> involved in the conversion processes did not originate from the wildfire

emissions. Rather, it points to the possible presence of additional NO<sub>x</sub> sources contributing to the loss reactions in these regions.

To investigate potential NO sources involved in these conversion processes, the horizontal and vertical distributions of anthropogenic NO<sub>x</sub> emissions used as input for the CMAQ model are presented in figure 5. In the NEC region, where reductions in NO<sub>x</sub> concentrations were observed (figure 2(b)), anthropogenic NO<sub>x</sub> was extensively emitted near the surface, whereas emissions in Siberia were relatively low (figure 5(a)). A substantial amount of NO<sub>x</sub> was also emitted vertically near the ABL over the NEC region (figure 5(b)), which is largely consistent with the vertical distribution of NO<sub>x</sub> concentration changes presented in figure 3(b). To assess whether these anthropogenic NO<sub>x</sub> emissions played a role in the NO<sub>x</sub> conversions, we conducted additional sensitivity experiments. We conducted three sensitivity simulations based on the BASE and SIB scenarios: NO<sub>x</sub>\_p30, in which anthropogenic NO<sub>x</sub>





emissions were increased by 30%; NO<sub>x</sub>\_m30, with emissions reduced by 30%; and NO<sub>x</sub>\_zero, where all anthropogenic NO<sub>x</sub> emissions were removed. The resulting changes in NO<sub>x</sub> concentrations were analyzed (figure S9). Interestingly, the spatial pattern of NO<sub>x</sub> concentration changes varied depending on the level of anthropogenic NO<sub>x</sub> emissions. The baseline simulation results (SIB-BASE) showed that NO<sub>x</sub> concentrations decreased by up to  $-4.07$  ppb (mean: 6.75%) during the EP2 period. In the NO<sub>x</sub>\_p30 experiment, the conversion became stronger, with a reduction of  $-4.88$  ppb (mean: 7.18%), whereas in the NO<sub>x</sub>\_m30 experiment, it weakened to  $-2.71$  ppb (mean: 5.90%). In the NO<sub>x</sub>\_zero experiment, where anthropogenic NO<sub>x</sub> emissions were entirely removed, the conversion processes disappeared, and no significant changes in NO<sub>x</sub> were observed. These results indicate that the conversion of NO<sub>x</sub> into NO<sub>3</sub> radicals, organic nitrates, and other species in the

NEC, YS, and KP regions became more pronounced with higher levels of anthropogenic NO<sub>x</sub> emissions, confirming that local emissions were the main driver of these transformations.

The findings of this study demonstrate that although wildfires can elevate pollutant concentrations near the source region, they do not necessarily lead to increases in all atmospheric pollutants in downwind areas. Instead, wildfire smoke plumes can interact with local anthropogenic emissions in these regions, triggering chemical processes that transform NO<sub>x</sub> into other species. Therefore, when wildfire-emitted smoke plumes are transported, it is essential to conduct detailed analyses of changes in gaseous pollutant concentrations, taking into account the nature of local emission sources. Such changes in gaseous pollutants may significantly influence the formation mechanisms of particulate matter (Clappier *et al* 2021,

Chuang *et al* 2022), highlighting the need for further investigation.

#### 4. Discussion

As noted in sections 2.3 and 3.1, the CMAQ model was unable to adequately reproduce CO concentrations due to the underestimation of CO in the anthropogenic emission inventory. To address this issue, we conducted sensitivity experiments in which anthropogenic CO emissions over China and South Korea were uniformly increased by factors of 2 and 3, respectively. The results showed that higher CO emissions led to much better agreement between simulation and observations. As CO emissions increased, the model showed better agreement with observed CO concentrations (figures S9 and S10). In particular, during the wildfire-affected days, the baseline simulation (figure S4(a)) considerably underestimated the observed CO levels, whereas the experiment with threefold CO emissions more effectively captured the wildfire-induced enhancement, leading to improved model performance (table S5). Nevertheless, the temporal variability was not well simulated, likely due to the uniform scaling of anthropogenic CO emissions across both China and South Korea in the sensitivity experiments. Importantly, this underestimation of CO does not affect the main findings and conclusions of this study. However, to reduce such uncertainties, future research should focus on improving the accuracy of anthropogenic CO emission inventories.

In addition, a key finding of this study is the conversion of NO<sub>x</sub> driven by O<sub>3</sub> and VOCs produced from the Siberian wildfires, which strongly depend on the amounts of NO<sub>x</sub> and VOCs emitted from the fires. According to the FINN inventory used in this study, the Siberian wildfires released  $1.28 \times 10^{10}$  mol d<sup>-1</sup> of NO<sub>x</sub> and  $1.33 \times 10^{11}$  mol d<sup>-1</sup> of VOCs. To quantitatively evaluate how changes in these emissions influence NO<sub>x</sub> concentrations in downwind regions, we conducted additional sensitivity experiments. Specifically, one experiment doubled the NO<sub>x</sub> emissions ( $2.56 \times 10^{10}$  mol d<sup>-1</sup>), while another reduced the VOC emissions to one-fourth of the baseline level ( $3.33 \times 10^{10}$  mol d<sup>-1</sup>). The increase in NO<sub>x</sub> emissions enhanced O<sub>3</sub> formation through photochemical reactions, resulting in greater O<sub>3</sub> transport toward the NEC, YS, and KP regions (figure S11(a)) and intensifying NO<sub>x</sub> conversion (−5.05 ppb) (figure S11(b)). In contrast, the reduction in VOC emissions not only decreased the amount of VOCs transported but also limited wildfire-induced O<sub>3</sub> production (figure S12(a)). Consequently, the extent of NO<sub>x</sub> concentration changes was mitigated (−2.68 ppb) (figure S12(b)). These results indicate that the NO<sub>x</sub> conversion processes in the NEC, YS, and KP regions are highly sensitive to the amounts of NO<sub>x</sub> and VOCs emitted from wildfires. Previous studies (Wiedinmyer *et al* 2011, Hodnebrog *et al* 2012, Naus

*et al* 2022) have reported that the FINN inventory tends to underestimate wildfire emissions. Therefore, accurate estimation of wildfire emissions is essential for quantitatively evaluating their atmospheric chemical impacts.

#### 5. Conclusions

In this study, we analyzed the concentration change characteristics of major gaseous pollutants (CO, NO<sub>x</sub>, VOCs, and O<sub>3</sub>) induced by wildfires that occurred in late July 2014 in Siberia, Russia. To investigate the air quality impacts of the wildfires, the three-dimensional photochemical model CMAQ was employed, with wildfire emissions extracted from the FINN (v2.5). A large amount of gaseous pollutants (CO, NO<sub>x</sub>, and VOCs) was emitted from the wildfires in the Siberian region, leading to the formation of O<sub>3</sub>. CO, VOCs, and O<sub>3</sub> were subsequently transported to downwind regions such as NEC, YS, and KP, resulting in elevated concentrations in those areas. However, NO<sub>x</sub> exhibited a distinct distribution compared to other species. Although wildfire plumes were transported from the Siberian region, surface-level NO<sub>x</sub> concentrations within the ABL decreased in downwind regions, including NEC, YS, and KP. These distributions of concentration reduction were not observed within the Siberian region, but, notably, began to appear after the smoke plume was transported to NEC. To investigate the spatial characteristics of this reduction, we employed the IRR module in the CMAQ model. The analysis revealed that NO was primarily converted through reactions with VOCs (84.54%) and NO<sub>3</sub> radicals (13.18%). Meanwhile, NO<sub>2</sub> was mostly transformed by O<sub>3</sub> (90.08%), and also participated in the formation of organic nitrates via reactions with VOCs (9.92%). These VOCs, O<sub>3</sub>, and NO<sub>3</sub> radicals induced by wildfires were transported to the NEC, YS, and KP regions, where they facilitated the chemical conversion of NO<sub>x</sub> into NO<sub>3</sub> radicals, organic nitrates, and other species. However, because NO<sub>x</sub> concentrations increased in Siberia due to wildfire emissions, the conversion patterns observed in the downwind regions cannot be explained solely by wildfire-emitted NO<sub>x</sub>. This implies the presence of NO<sub>x</sub> sources in NEC, YS, and KP that could react with VOCs, O<sub>3</sub>, and NO<sub>3</sub> radicals. Through additional sensitivity experiments, we confirmed that the NO<sub>x</sub> involved in the chemical transformations originated from anthropogenic sources. Compared to Siberia, substantial anthropogenic NO<sub>x</sub> emissions were present in the NEC, YS, and KP regions, where the transported smoke plume facilitated the chemical conversion of these locally emitted NO<sub>x</sub>. Such a conversion pattern disappeared when anthropogenic NO<sub>x</sub> emissions were excluded.

This study found that interactions between wildfire plumes and local anthropogenic emissions can induce complex chemical processes that convert NO<sub>x</sub>

into other species. These findings contrast with the conventional understanding that wildfire emissions generally increase pollutant concentrations in down-wind regions. Given that such chemical transformations in gaseous species may significantly affect the formation mechanisms of secondary particulate matter, it is important to consider changes in gaseous pollutant concentrations in conjunction with the characteristics of local emission sources during wildfire events. These results suggest that emission control policies should take into account not only regional emission characteristics but also the interactions between existing anthropogenic sources and wildfire emissions. Accordingly, we expect that the findings of this study will serve as a valuable reference for predicting the spatial distribution and behavior of air pollutants in future wildfire-related research.

### Data availability statement


All data that support the findings of this study are included within the article (and any supplementary files).

Supplementary Information available at <https://doi.org/10.1088/1748-9326/ae2526/data1>.

### Acknowledgment

This work was supported by the National Research Foundation of Korea (NRF) grant funded by the Korea Government (MSIT) (No. RS-2023-NR076349) and the Basic Science Research Program through the National Research Foundation of Korea (NRF) funded by the Ministry of Education (RS-2020-NR049592).


### Author contributions

Dongjin Kim  0000-0003-3562-0384  
Conceptualization (equal), Formal analysis (equal), Investigation (lead), Methodology (equal), Writing – original draft (lead)

Yunsoo Choi  
Supervision (supporting), Writing – review & editing (equal)

Hyun Cheol Kim  0000-0003-3968-6145  
Writing – review & editing (equal)

Arman Pouyaei  0000-0002-0128-0572  
Writing – review & editing (equal)

Jaehyeong Park  0000-0001-6359-5396  
Investigation (equal), Validation (equal), Writing – review & editing (equal)

Jeonghyeok Moon  0000-0002-4050-1024  
Resources (equal), Software (equal)

Chae-Yeong Yang  0009-0006-6173-0412  
Writing – review & editing (supporting)

Cheol-Hee Kim  0000-0002-2967-4987

Funding acquisition (equal)

Wonbae Jeon  0000-0002-4898-7292

Conceptualization (equal), Formal analysis (equal), Project administration (lead), Supervision (lead), Writing – review & editing (lead)

### References

- Appel K et al 2021 The Community Multiscale Air Quality (CMAQ) model versions 5.3 and 5.3.1: system updates and evaluation *Geosci. Model. Dev.* **14** 2867–97
- Baylon P, Jaffe D A, Wigder N L, Gao H and Hee J 2015 Ozone enhancement in western US wildfire plumes at the Mt. Bachelor observatory: the role of NO<sub>x</sub> *Atmos. Environ.* **109** 297–304
- Bieser J, Aulinger A, Matthias V, Quante M and Denier van der Gon H A C 2011 Vertical emission profiles for Europe based on plume rise calculations *Environ. Pollut.* **159** 2935–46
- Byun D W and Ching J K S 1999 *Science Algorithms of the EPA Models-3 Community Multiscale Air Quality (CMAQ) Modeling System* (U.S. Environmental Protection Agency, NERL, Research Triangle Park)
- Chance K 2007 OMI/Aura formaldehyde (HCHO) total column 1-orbit L2 swath 13x24 km (available at: <https://10.5067/Aura/OMI/DATA2015>)
- Chuang M-T, Wu C-F, Lin C-Y, Lin W-C, Chou C C-K, Lee C-T, Lin T-H, Fu J S and Kong S S-K 2022 Simulating nitrate formation mechanisms during PM<sub>2.5</sub> events in Taiwan and their implications for the controlling direction *Atmos. Environ.* **269** 118856
- Clappier A, Thunis P, Beekmann M, Putaud J P and de Meij A 2021 Impact of SO<sub>x</sub>, NO<sub>x</sub> and NH<sub>3</sub> emission reductions on PM<sub>2.5</sub> concentrations across Europe: hints for future measure development *Environ. Int.* **156** 106699
- Crippa M, Guizzardi D, Muntean M, Schaaf E, Monforti-Ferrario F, Banja M, Pegani F and Solazzo E 2022 EDGAR v6.1 global air pollutant emissions (available at: <https://publications.jrc.ec.europa.eu/repository/handle/JRC129555>)
- Dreessen J, Sullivan J and Delgado R 2016 Observations and impacts of transported Canadian wildfire smoke on ozone and aerosol air quality in the Maryland region on June 9–12, 2015 *J. Air Waste Manage. Assoc.* **66** 842–62
- Feng S, Jiang F, Wu Z, Wang H, Ju W and Wang H 2020 CO emissions inferred from surface CO observations over China in December 2013 and 2017 *J. Geophys. Res.* **125** e2019JD031808
- Guenther A B, Jiang X, Heald C L, Sakulyanontvittaya T, Duhl T, Emmons L K and Wang X 2012 The model of emissions of gases and aerosols from nature version 2.1 (MEGAN2.1): an extended and updated framework for modeling biogenic emissions *Geosci. Model. Dev.* **5** 1471–92
- Hansen M et al 2013 High-resolution global maps of 21st-century forest cover change *Science* **342** 850–3
- Hodnebrog Ø et al 2012 Impact of forest fires, biogenic emissions and high temperatures on the elevated Eastern Mediterranean ozone levels during the hot summer of 2007 *Atmos. Chem. Phys.* **12** 8727–50
- Huang Y, Lu X, Fung J C H, Wong D C, Li Z, Chen Y and Chen W 2023 Investigating Southeast Asian biomass burning by the WRF-CMAQ two-way coupled model: emission and direct aerosol radiative effects *Atmos. Environ.* **294** 119521
- Ikeda K and Tanimoto H 2015 Exceedances of air quality standard level of PM<sub>2.5</sub> in Japan caused by Siberian wildfires *Environ. Res. Lett.* **10** 105001
- Jeon W, Choi Y, Souri A H, Roy A, Diao L, Pan S, Lee H W and Lee S-H 2018 Identification of chemical fingerprints in long-range transport of burning induced upper



- tropospheric ozone from Colorado to the North Atlantic Ocean *Sci. Total Environ.* **613–14** 820–8
- Jeong J I, Park R J and Youn D 2008 Effects of Siberian forest fires on air quality in East Asia during May 2003 and its climate implication *Atmos. Environ.* **42** 8910–22
- Jo H-Y et al 2023 Interpretation of the effects of anthropogenic chlorine on nitrate formation over northeast Asia during KORUS-AQ 2016 *Sci. Total Environ.* **894** 164920
- Jung J, Lyu Y, Lee M, Hwang T, Lee S and Oh S 2016 Impact of Siberian forest fires on the atmosphere over the Korean Peninsula during summer 2014 *Atmos. Chem. Phys.* **16** 6757–70
- Kang C-M, Gold D and Koutrakis P 2014 Downwind O<sub>3</sub> and PM<sub>2.5</sub> speciation during the wildfires in 2002 and 2010 *Atmos. Environ.* **95** 511–9
- Kim D, Choi Y, Jeon W, Mun J, Park J, Kim C-H and Yoo J-W 2024 Quantitative analysis of sulfate formation from crop burning in Northeast China: unveiling the primary processes and transboundary transport to South Korea *Atmos. Res.* **302** 107303
- Kim D, Jeon W, Park J, Mun J, Choi H, Kim C-H, Lee H-J and Jo H-Y 2022a A numerical analysis of the changes in O<sub>3</sub> concentration in a wildfire plume *Remote Sens.* **14** 4549
- Kim H et al 2022b Observed versus simulated OH reactivity during KORUS-AQ campaign: implications for emission inventory and chemical environment in East Asia *Elem. Sci. Anth.* **10** 00030
- Krotkov N A et al 2024 OMI/Aura nitrogen dioxide (NO<sub>2</sub>) total and tropospheric column 1-orbit L2 swath 13x24 km (available at: <https://10.5067/Aura/OMI/DATA2417>)
- Li X, Xia X, Song J, Wu Y, Zhang X and Zhang R 2017 A case study of long-range transport of smoke aerosols Eastern Siberia to Northeast China in July 2014 *Aerosol Air Qual. Res.* **17** 965–74
- Li Y et al 2023 Impacts of estimated plume rise on PM<sub>2.5</sub> exceedance prediction during extreme wildfire events: a comparison of three schemes (Briggs, Freitas, and Sofiev) *Atmos. Chem. Phys.* **23** 3083–101
- Majdi M, Sartelet K, Lanzafame G M, Couvidat F, Kim Y, Chrit M and Turquety S 2019 Precursors and formation of secondary organic aerosols from wildfires in the Euro-Mediterranean region *Atmos. Chem. Phys.* **19** 5543–69
- Mazzeo A, Zhong J, Hood C, Smith S, Stocker J, Cai X and Bloss W J 2022 Modeling the impact of national vs. local emission reduction on PM<sub>2.5</sub> in the West Midlands, UK using WRF-CMAQ *Atmosphere* **13** 377
- Mun J et al 2023 Assessing mass balance-based inverse modeling methods via a pseudo-observation test to constrain NO<sub>x</sub> emissions over South Korea *Atmos. Environ.* **292** 119429
- Naus S et al 2022 Sixteen years of MOPITT satellite data strongly constrain Amazon CO fire emissions *Atmos. Chem. Phys.* **22** 14735–50
- Otte T L and Pleim J E 2010 The Meteorology-Chemistry Interface Processor (MCIP) for the CMAQ modeling system: updates through MCIPv3.4.1 *Geosci. Model. Dev.* **3** 243–56
- Park J, Jeon W, Mun J and Kim D 2021 A quantitative analysis of the effect of ocean emissions on the simulated ozone concentration in South Korea *J. Environ. Sci. Int.* **30** 413–24
- Park J, Jung J, Choi Y, Mousavinezhad S and Pouyaei A 2022 The sensitivities of ozone and PM<sub>2.5</sub> concentrations to the satellite-derived leaf area index over East Asia and its neighboring seas in the WRF-CMAQ modeling system *Environ. Pollut.* **306** 119419
- Park J, Mun J, Kim D, Lee H W, Kim C-H, Lee H-J, Jo H-Y, Koo J-Y, Choe H and Jeon W 2024 Assessing the impact of shipping emissions on ozone concentrations in East Asia: insights from KORUS-AQ and SIJAQ 2021. Campaign periods *Atmos. Environ.* **320** 120339
- Paugam R, Wooster M, Freitas S and Val Martin M 2016 A review of approaches to estimate wildfire plume injection height within large-scale atmospheric chemical transport models *Atmos. Chem. Phys.* **16** 907–25
- Pouyaei A, Ginoux P, Ward D S, Yu Y and Horowitz L W 2025 Implementation of dynamic fire injection height in GFDL's atmospheric model (AM4.0): impacts on aerosol profiles and radiation *J. Adv. Model. Earth Syst.* **17** e2024MS004407
- Raffuse S M, Craig K J, Larkin N K, Strand T T, Sullivan D C, Wheeler N J M and Solomon R 2012 An evaluation of modeled plume injection height with satellite-derived observed plume height *Atmosphere* **3** 103–23
- Skamarock W C et al 2019. A description of the advanced research WRF model version 4. *National Center for Atmospheric Research: Boulder, CO, USA* 145
- Sofiev M, Ermakova T and Vankevich R 2012 Evaluation of the smoke-injection height from wild-land fires using remote-sensing data *Atmos. Chem. Phys.* **12** 1995–2006
- Souri A H, Choi Y, Jeon W, Kochanski A K, Diao L, Mandel J, Bhawe P and Pan S 2017 Quantifying the impact of biomass burning emissions on major inorganic aerosols and their precursors in the U.S *J. Geophys. Res. Atmos.* **122** 12020–41
- Sun K et al 2018 A physics-based approach to oversample multi-satellite, multispecies observations to a common grid *Atmos. Meas. Tech.* **11** 6679–701
- Tang Z, Chen J and Jiang Z 2022 Discrepancy in assimilated atmospheric CO over East Asia in 2015–2020 by assimilating satellite and surface CO measurements *Atmos. Chem. Phys.* **22** 7815–26
- Trieu T T N, Morino I, Uchino O, Tsutsumi Y, Izumi T, Sakai T, Shibata T, Ohyama H and Nagahama T 2023 Long-range transport of CO and aerosols from Siberian biomass burning over northern Japan during 18–20 May 2016 *Environ. Pollut.* **322** 121129
- Urbanski S P, Hao W M and Baker S 2008 Chemical composition of wildland fire emissions *Dev. Environ. Sci.* **8** 79–107
- Val Martin M, Logan J A, Kahn R A, Leung F-Y, Nelson D L and Diner D J 2010 Smoke injection heights from fires in North America: analysis of 5 years of satellite observations *Atmos. Chem. Phys.* **10** 1491–510
- Wiedinmyer C et al 2023 The fire inventory from NCAR version 2.5: an updated global fire emissions model for climate and chemistry applications *Geosci. Model. Dev.* **16** 3879–91
- Wiedinmyer C, Akagi S K, Yokelson R J, Emmons L K, Al-Saadi J A, Orlando J J and Soja A J 2011 The fire inventory from NCAR (FINN): a high resolution global model to estimate the emissions from open burning *Geosci. Model. Dev.* **4** 625–41
- Xie Y, Han H and Liu J 2025 Spatial and seasonal variations and trends in carbon monoxide over China during 2013–2022 *Atmos. Environ.* **350** 121163
- Zhu C, Kanaya Y, Yoshikawa-Inoue H, Irino T, Seki O and Tohjima Y 2019 Sources of atmospheric black carbon and related carbonaceous components at Rishiri Island, Japan: the roles of Siberian wildfires and of crop residue burning in China *Environ. Pollut.* **247** 55–63